
GRAPHLCP: Structure-Aware Localized Conformal Prediction on Graphs

Peyman Baghersahi¹ Fangxin Wang¹ Debmalya Mandal² Sourav Medya¹

¹Department of Computer Science, University of Illinois Chicago

²Department of Computer Science, University of Warwick

¹{pbaghe2, fwang51, medya}@uic.edu; ²debmalya.mandal@warwick.ac.uk

Abstract

Conformal prediction (CP) provides a distribution-free approach to uncertainty quantification with finite-sample guarantees. However, applying CP to graph neural networks (GNNs) remains challenging as the combinatorial nature of graphs often leads to insufficiently certain predictions and indiscriminative embeddings. Existing methods primarily rely on embedding-space proximity for localization, which can be unreliable for graphs and yield inefficient prediction sets. We propose GRAPHLCP, a proximity-based localized CP framework that explicitly incorporates graph topology and inter-node dependencies into localization and weighting. Our approach introduces a feature-aware densification step to mitigate locality bias in sparse graphs, followed by a Personalized PageRank-based kernel computation to model structural proximity. This enables topology-dependent anchor sampling and calibration weighting that captures both local and long-range dependencies. Extensive experiments on several regression and classification datasets demonstrate that GRAPHLCP guarantees marginal coverage with finite samples while efficiently attaining favorable test conditional coverage across various conditioning scenarios.

1 Introduction

Graph neural networks (GNNs) are increasingly deployed for drug discovery [8], weather prediction [29], and fraud detection in financial networks [6]. In these high-stakes applications, relying solely on point predictions is risky and the practitioners require reliable uncertainty quantification (UQ) of GNNs to assess the trustworthiness of predictions. Conformal Prediction (CP) is an effective distribution-free framework for constructing set-valued predictions that guarantees covering the ground-truth values using a finite sample of data points [36, 1]. Consequently, CP has emerged as a widely adopted approach for post-hoc reliability, applied to graph tasks such as standard regression, link prediction, and out-of-distribution detection [26, 30, 47].

Classical CP guarantees *marginal* coverage on average over the test distribution. However, in many practical settings, uncertainty is heterogeneous, requiring reliability specific to subpopulations or local contexts [34, 5]. Achieving *exact* conditional coverage per sample is known to be impossible in finite samples [9]. This limitation has motivated a growing body of work on *relaxed* notions of conditional coverage, leveraging localization and weighting strategies to improve validity [41, 2]. A central requirement across these approaches is the availability of a meaningful notion of *proximity* between the test sample and the calibration data.

In graphs, predictive reliability varies across regions with different homophily patterns [7]. Besides, applying CP on graphs is challenging because nodes are naturally dependent, violating standard i.i.d assumptions [27, 7]. In practice, CP for GNNs often leverages the embedding space, using learned representations as proxies for instances [25]. However, this proxy can be unreliable as message passing can suffer from a graph-topological bottleneck (over-squashing), restricting global

information flow and exacerbating noise under heterophily [13]. Meanwhile, deeper message passing causes over-smoothing, reducing the variance of similarity measures [35]. Also, GNNs generally exhibit under-confidence, suggesting insufficient separability in the learned representation [43, 17]. These effects complicate the core requirement of having a stable proximity kernel for localized CP, which reweights calibration data based on their similarity to the test instance [16].

Recent work has extended conformal prediction to GNNs to address structural dependencies, with approaches ranging from handling inductive covariate shift [45, 7] to developing diffusion-based scores [44]. Built on findings which preserve exchangeability under permutation-invariant transformation [24, 27, 28], recent studies have also applied CP to GNNs in transductive settings [18, 46]. Additional related work is provided in the Appendix A.1.

However, several limitations remain in the existing approaches. A few methods rely on training auxiliary models to calibrate residuals [18, 46] or fine-tuning the base predictor [25]. These increase computational overhead and reduce sample efficiency by necessitating data splitting, effectively deviating from the lightweight, post-hoc nature that makes CP useful. Also, the methods based on localized CP typically rely either on *embedding-space* weighting (e.g., kernel density estimation) [25] or on *purely structural* partitioning (e.g., hard clustering of communities) [46]. These strategies can be fragile because embedding-based similarities may become indiscriminative due to smoothing, while rigid structural clusters may fail to capture fine-grained local heterophily in graphs. As a result, existing graph CP methods typically perform best under strong homophily and may yield overly conservative or poorly *localized prediction sets* in complex topologies.

In this work, we bridge the gap between structural and feature-based localization. We propose GRAPHLCP, a proximity-based localized CP framework for GNNs that explicitly incorporates graph topology and inter-node dependencies into localization-based weighting for conformal quantile computation. Our approach replaces embedding-only proximity with a structure-aware proximity kernel based on Personalized PageRank (PPR), enabling topology-dependent anchor sampling and calibration weighting. To mitigate locality bias in sparse graphs and capture long-range dependencies, we introduce a feature-aware densification step that augments the graph using embedding similarity prior to kernel computation. Together, these enable GRAPHLCP to maintain marginal coverage while achieving efficient approximate conditional coverage across node-level regression and classification tasks. Through experiments on *seven regression* and *eight classification* datasets, we demonstrate the efficacy of GRAPHLCP based on marginal coverage and favorable approximate conditional coverage, with efficient prediction length (size).

2 Preliminaries and Problem Setup

2.1 Graph Neural Network (GNN)

In this work, we focus on the canonical form of GNNs, which use a message-passing mechanism. We denote a graph as $\mathcal{G}(\mathcal{V}, \mathbf{A}, \mathbf{X})$ where \mathcal{V} is the set of vertices or nodes with $|\mathcal{V}| = N_G$; $\mathbf{X} \in \mathbb{R}^{N_G \times d}$ and $\mathbf{A} \in \{0, 1\}^{N_G \times N_G}$ are the features and the adjacency matrix of the graph. According to [11], an L -layer pre-trained message-passing model ϕ derives a node’s l -th layer state or representation, $\mathbf{x}_u^{(l)}$ ($\forall u \in \mathcal{V}, l \leq L$) using three functions – (i) a *message-passing* function M_ϕ that propagates the l -th layer state of every node in the neighborhood $\mathcal{N}_u = \{v : v \in \mathcal{V}, \mathbf{A}_{uv} = 1\}$, (ii) an *aggregate function* C_ϕ to combine the messages from M_ϕ , and (iii) an *update function* U_ϕ to derive the node’s latest state integrating its $(l - 1)$ -th layer state and the aggregated message. Formally,

$$\mathbf{x}_u^{(l)} = U_\phi(C_\phi(\{M_\phi(\mathbf{x}_v^{(l)}); v \in \mathcal{N}_u\}), \mathbf{x}_u^{(l-1)}).$$

Given a downstream task, most GNNs use a simple function (e.g., a linear neural network) to decode the latest embeddings or states to prediction logits as $\hat{y}_u = f(\mathbf{x}_u^{(L)})$. Also, for the ease of notation, we use: $\mathbf{x}_i : \forall i \in [N_G]$ instead of $\mathbf{x}_u^{(L)} : \forall u \in \mathcal{V}$, and also y_i instead of \hat{y}_u for $i \in [N_G]$.

In contrast to standard conformal prediction, where samples are assumed to be exchangeable, conformal validity on graphs is not trivial because node samples are generally dependent, particularly in inductive settings. However, in the node-level transductive setting with a random train/calibration/test split, calibration and test nodes remain exchangeable as long as their labels are not used during training. Once the GNN is trained and frozen, it induces a deterministic transformation from each node and its topological context to an embedding representation, which is then used for conformal

prediction. Since conventional GNNs are permutation equivariant and the resulting nonconformity scores are permutation-invariant with respect to calibration and test node permutations, standard conformal prediction guarantees marginal node-level coverage under this transductive setup [18, 27].

2.2 Conformal Prediction (CP)

Split Conformal Prediction (SCP). Given a dataset $\mathcal{D} = \{(\mathbf{x}_i, y_i) : (\mathbf{x}_i, y_i) \sim \mathcal{P} = \mathcal{P}_X \times \mathcal{P}_{Y|X}, \mathbf{x}_i \in \mathcal{X}, y_i \in \mathcal{Y}\}_{i=1}^{N_G}$ (e.g., \mathbf{x}_i are the nodes or their embeddings), we first split the dataset to three disjoint sets: 1) \mathcal{D}_{tr} with labels for supervised training, 2) \mathcal{D}_{cal} with labels as holdout calibration set, and 3) \mathcal{D}_{test} purposefully made without labels as test point. After training the message-passing (ϕ) and decoder (f) modules on \mathcal{D}_{tr} , we freeze the model for CP. Having n labeled samples $\{z_i = (\mathbf{x}_i, y_i) \in \mathcal{D}_{cal} : \forall i \in [n]\}$, the problem is to construct a prediction interval $\hat{C}_n(\mathbf{x}_{n+1})$ for an unlabeled sample $\mathbf{x}_{n+1} \in \mathcal{D}_{test}$ that contains or ‘‘covers’’ the groundtruth label y_{n+1} of the test sample with probability at least $1 - \alpha$, where α is the miscoverage rate.

In order to achieve the desired coverage, every calibration sample and the test sample are assigned a non-conformity as $S_i = s(\mathbf{x}_i, y_i), \forall i \in [n]$ and $S_{n+1} = s(\mathbf{x}_{n+1}, y) : y \in \mathcal{Y}$, where $s(x, y)$ is a non-conformity score function. For example, absolute residual, $s(x, y) = |y - f(x)|$, is a commonly used function. Additionally, let $\hat{q} = \text{Quantile}_{1-\alpha}(\sum_{i=1}^n \frac{1}{n+1} \delta_{s(z_i)} + \frac{1}{n+1} \delta_{+\infty})$, where δ_x is the probability distribution that places probability 1 on the value x , and 0 everywhere else. If S_{n+1} is exchangeable with $\{S_i\}_{i=1}^n$, then by constructing $\hat{C}_n(\mathbf{x}_{n+1}) = \{y \in \mathcal{Y} : s(\mathbf{x}_{n+1}, y) \leq \hat{q}\}$ we have $\mathbb{P}\{y_{n+1} \in \hat{C}_n(\mathbf{x}_{n+1})\} \geq 1 - \alpha$ [42]. This, being averaged over all random draws of the calibration and the test samples, is called *marginal coverage*. However, if the coverage is guaranteed for every specific instance of \mathbf{x}_{n+1} , it is called *conditional coverage*, requiring $\mathbb{P}\{y_{n+1} \in \hat{C}_n(\mathbf{x}_{n+1}) \mid \mathbf{x}_{n+1}\} \geq 1 - \alpha$. [9] shows that achieving such test conditional coverage is infeasible. Therefore, test conditional coverage is commonly relaxed and measured for a test sample $\mathbf{x}_{n+1} \in B$ where $B \in \mathcal{B}$ and \mathcal{B} is a collection of subsets of feature space, i.e. $B \subseteq \mathcal{X}$, and the guarantee requires $\mathbb{P}\{y_{n+1} \in \hat{C}_n(\mathbf{x}_{n+1}) \mid \mathbf{x}_{n+1} \in B : B \in \mathcal{B}\} \geq 1 - \alpha$.

Weighted Conformal Prediction (WCP). Weighted Conformal Prediction (WCP) is one of the ways to attain the above notion of relaxed test conditional coverage [41]. Suppose we are given a kernel function $H(\mathbf{x}, \mathbf{x}')$, e.g. $H(\mathbf{x}, \mathbf{x}') = \frac{1}{(2\pi h^2)^{d/2}} \exp\left(-\frac{\|\mathbf{x}-\mathbf{x}'\|_2^2}{2h^2}\right)$. Then we can apply WCP for local coverage by using the kernel centered at $\mathbf{x} = \mathbf{x}_{n+1}$, and obtain coverage for a nearby (synthetic) sample $\tilde{\mathbf{x}}_{n+1} = \mathbf{x}_{n+1} + h \cdot \mathbf{w}$ s.t. $\mathbf{w} \sim H(\mathbf{x}_{n+1}, \cdot)$, but not necessarily for \mathbf{x}_{n+1} itself, i.e. $\mathbb{P}\{y_{n+1} \in \hat{C}_n(\tilde{\mathbf{x}}_{n+1}) \mid \mathbf{x}_{n+1} = \tilde{\mathbf{x}}_{n+1} + h \cdot \mathbf{w}\} \geq 1 - \alpha$. This locally-weighted method, for some small bandwidth h , approximately guarantees exact coverage at \mathbf{x}_{n+1} .

Randomly Localized Conformal Prediction (RLCP). Unlike WCP, the Randomly Localized Conformal Prediction (RLCP) method [16] guarantees relaxed test conditional coverage for the test sample $\tilde{\mathbf{x}}_{n+1}$, rather than a point $\tilde{\mathbf{x}}_{n+1}$ in its proximity. RLCP simply applies WCP to a randomly sampled point $\tilde{\mathbf{x}}_{n+1}$ in the proximity of \mathbf{x}_{n+1} , i.e. $\tilde{\mathbf{x}}_{n+1} \mid \mathbf{x}_{n+1} \sim H(\mathbf{x}_{n+1}, \cdot)$, which ensures $\mathbb{P}\{Y_{n+1} \in \hat{C}_n^{\text{RLCP}}(\mathbf{x}_{n+1}, \tilde{\mathbf{x}}_{n+1})\} \geq 1 - \alpha$.

Suppose there is a kernel function as $H : \mathcal{X} \times \mathcal{X} \rightarrow \mathbb{R}_{\geq 0}$ such that $\int_{\mathcal{X}} H(x, x') dv(x') = 1, \forall x \in \mathcal{X}$. Now, for a test sample $(\mathbf{x}_{n+1}, Y_{n+1})$ exchangeable with the calibration samples $(\mathbf{x}_i, Y_i) : i \in [n]$, RLCP samples an anchor point $\tilde{\mathbf{x}}_{n+1} \sim \mathcal{P}_{\mathbf{x}} \circ H(\cdot, \mathbf{x}_{n+1})$ and construct the CP interval/set of \mathbf{x}_{n+1} as $\hat{C}_n^{\text{RLCP}}(\mathbf{x}_{n+1}, \tilde{\mathbf{x}}_{n+1}) = \{y \in \mathcal{Y} : s(\mathbf{x}_{n+1}, y) \leq \hat{q}_{1-\alpha}(\mathbf{x}_{n+1}, \tilde{\mathbf{x}}_{n+1})\}$ where

$$\hat{q}_{1-\alpha}(\mathbf{x}_{n+1}, \tilde{\mathbf{x}}_{n+1}) = \text{Quantile}_{(1-\alpha)} \sum_{i=1}^n \tilde{w}_i \delta_{s(z_i)} + \tilde{w}_{n+1} \delta_{+\infty} \quad (1)$$

and the weights are derived as $\tilde{w}_i = \frac{H(\mathbf{x}_i, \tilde{\mathbf{x}}_{n+1})}{\sum_{j=1}^{n+1} H(\mathbf{x}_j, \tilde{\mathbf{x}}_{n+1})}$.

Our Objective. We address the problem of CP for GNNs by explicitly incorporating structural proximity into the weighting step. By decoupling weights from potentially lossy encoders, we create a lower-noise residual pathway that leverages embedding proximity while controlling its influence. *Our goal is to satisfy marginal coverage with efficient prediction interval sizes while achieving strong test conditional coverage.* We motivate this with an empirical analysis (Appendix A.2) of the

existing embedding-based localized methods (e.g., RLCP) failing for GNNs because indiscriminative embeddings cause feature-based proximity weights to collapse into non-informative extremes. This either completely isolates the test point or reduces to a uniform standard CP.

3 Our Method: GRAPHLCP

Recent studies attempted to incorporate structural covariates into GNN-based conformal prediction (CP) [7, 46], yet they have failed to significantly improve conditional coverage. While graph structures are implicitly encoded in GNN embeddings, lossy encoders or sparse topologies can create bottlenecks, and over-smoothing in denser graphs often diminishes topological dependencies [12, 33, 35]. To mitigate this, we propose GRAPHLCP, a structure-aware CP method that ensures marginal coverage while achieving high relaxed test conditional coverage. Our approach utilizes a localized kernel and a weighting strategy, illustrated in Figure 1, which remains resilient to embedding suboptimality by explicitly incorporating underlying structural dependencies (empirical evidence demonstrating the strong correlation between node homophily and coverage is provided in Appendix A.3).

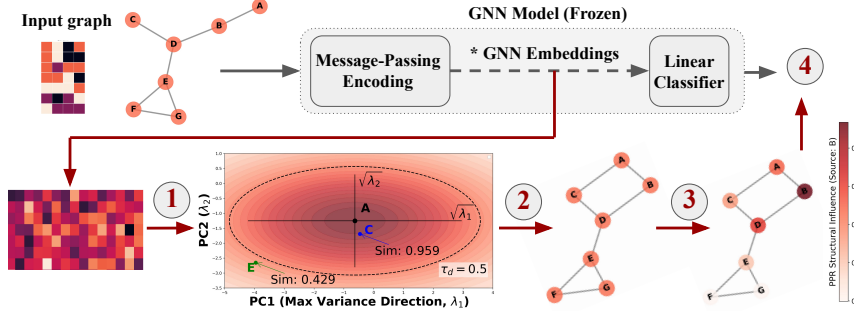


Figure 1: **GRAPHLCP**. Given the embeddings of a frozen GNN for an input graph, GRAPHLCP goes through four stages: 1) **PCA Transformation**: high-dimensional embeddings are decorrelated and largest eigenvalues (corresponding to directions of highest variance) yield an adaptive bandwidth for an anisotropic Gaussian kernel; 2) **Graph Densification**: adding informative edges via a homophily-based dynamic threshold; 3) **PPR Integration**: utilizing the PPR kernel to sample anchor nodes (for each test sample) and weight calibration samples; and 4) **Conformal Prediction**: a weighted quantile is computed from calibration samples to construct the final prediction set/interval.

3.1 Sampling and Weighting with Personalized PageRank (PPR)

To model structural proximity, we adopt Personalized PageRank (PPR) [19] as our localization kernel. PPR captures multi-hop influence while maintaining locality via a restart probability, effectively modeling uncertainty propagation in heterogeneous graphs [32]. Unlike shortest-path or k-hop neighborhoods, PPR provides a soft, probabilistic notion of proximity that naturally aligns with weighted CP. Importantly, PPR yields a valid probability distribution over nodes, allowing it to be directly used as a randomized localization kernel compatible with RLCP.

PPR is formally defined as $\pi = \beta s(I - (1 - \beta)M)^{-1}$, where β is the restart/teleportation probability, s is the seed distribution vector, with $\sum_{i=1}^{|\mathcal{V}|} [s]_i = 1$, and $M = D^{-1}A$ is the transition matrix, with D being the diagonal degree matrix. Let e_i be a one-hot vector, s.t. $[e_i]_i = 1$ and $[e_i]_j = 0 : \forall j \in \mathcal{V}, i \neq j$. For a seed node u_i , denoted as π_i , PPR yields a vector representing the stationary distribution of a random walk that, at each step, restarts at u_i with probability β . The value $[\pi_i]_j$ denotes the long-run probability of the walk being at node u_j if started at node u_i . Since, we have to use the kernel both for sampling and weighting, we use a compatible definition of PPR. Let $k \sim \text{Geom}(\beta)$ be the length of a random walk sampled from a geometric distribution $\text{Geom}(\beta)$, where β is the probability of success (e.g., restart probability). The PPR vector is the expected position of a random walker after k steps:

$$\pi = \mathbb{E}_{L \sim \text{Geom}(\beta)} [sM^k] = \sum_{k=0}^{\infty} \beta(1 - \beta)^k sM^k \quad (2)$$

Using the power iteration method, [10] approximates the above PPR by K iterations rather than infinite summation so we have $\boldsymbol{\pi}^{(k)} = (1 - \beta)\mathbf{M}\boldsymbol{\pi}^{(k-1)} + \beta\mathbf{s}$, and this converges to exact PPR once $K \rightarrow \infty$. Finally, we have $\boldsymbol{\pi} \simeq \boldsymbol{\pi}^{(K)}$.

The above definition helps us sample from the distribution induced by $\boldsymbol{\pi}_u$ with node u as the seed. We decompose sampling the anchor nodes into two independent steps. *First*, we sample a random walk length $k \sim \text{Geom}(\beta)$. *Second*, we chose the landing node the k -step random walk starting from u . Moreover, because we use the method in [10] to estimate the PPR vectors, we also avoid random walks beyond K steps during sampling. This imposes a loss of probability mass $(1 - \beta)^{K+1}$, which is negligible for a sufficiently large value of K or β , e.g. in our experiments, we fix $K = 30$.

Anchor Sampling. Analogous to RLCP, in graph space, we construct prediction sets by sampling an anchor node in the neighborhood of the test node and computing conformal scores relative to this anchor. In GRAPHLCP, anchor nodes are sampled from the PPR-induced distribution centered at the test node, so the nearby nodes exert greater influence on the quantile estimation. Given a test node u_{n+1} , we sample the anchor node as $\tilde{u}_{n+1}|u_{n+1} \sim H(u_{n+1}, \cdot)$. Replacing $H(u_{n+1}, \cdot)$ with distribution $\boldsymbol{\pi}_{n+1}$, for the seed vector \mathbf{s}_{n+1} one-hot at u_{n+1} we have:

$$\tilde{u}_{n+1}|u_{n+1} \sim H(u_{n+1}, \cdot) \rightarrow \tilde{u}_{n+1}|u_{n+1} \sim \boldsymbol{\pi}_{n+1} \quad (3)$$

Structural Weighting. Once the anchor node is sampled, calibration and test nodes are weighted according to their structural proximity to the anchor. Unlike Gaussian kernels, PPR is asymmetric, meaning structural influence is direction-dependent. Essentially, we have $H(u_i, u_j) \neq H(u_j, u_i)$, and $\tilde{w}_i \sim H(u_i, \tilde{u}_{n+1})$ which requires computing $\boldsymbol{\pi}_i : \forall i \in [n]$. In cases where we have n calibration samples and m test samples s.t. $n < m$, it is efficient to compute $\boldsymbol{\pi}_i : \forall i \in [n]$ directly. However, when $n > m$ (e.g., in a single-sample/pointwise case), this approach is inefficient. To resolve this issue for undirected graphs, we compute weights efficiently by exploiting the degree-normalized symmetry property of PPR, such that $d_i H(u_i, u_j) = d_j H(u_j, u_i)$, where d_i denotes the degree of node u_i . To keep the consistency of notation, we write $d_i[\boldsymbol{\pi}_i]_j = d_j[\boldsymbol{\pi}_j]_i$. Letting $\tilde{\boldsymbol{\pi}}_{n+1}$ denote the PPR-based induced distribution with sampled anchor \tilde{u}_{n+1} as the center, the calibration and test nodes are weighted according to the anchor node as follows

$$\tilde{w}_i = \frac{d_i^{-1}[\tilde{\boldsymbol{\pi}}]_i}{\sum_{j=1}^{n+1} d_j^{-1}[\tilde{\boldsymbol{\pi}}]_j}, \quad \forall i \in [n+1] \quad (4)$$

Intuitively, nodes that exert stronger structural influence on the anchor node contribute more to the conformal quantile, adapting the graph context. This topological control of nodes' contributions particularly helps with conditional coverage by filtering out noisy information and focusing on structurally proximal nodes.

Remark. While the PPR-based kernel effectively captures structural similarity between nodes, it does not incorporate node attributes. At the same time, although GNN embeddings are imperfect and can be noisy due to information bottlenecks and over-smoothing, they determine the prediction logits and therefore remain an important source of information for uncertainty quantification. In addition, the PPR-based proximity measure behaves differently depending on graph density. In dense graphs, PPR explores many paths via random walks and captures global structure, whereas in sparse graphs it performs poorly due to strong localization [31], since the random walk probability mass drops rapidly, leading to negligible scores for distant nodes. This causes biased or overly localized weighting.

To address these limitations, we introduce a feature-aware graph densification step prior to PPR kernel computation. This augments the topology with embedding similarity, mitigating the inherent localization bias and allowing the random walk to bridge sparse regions and capture long-range semantic dependencies. We note that GNN over-smoothing collapses the embedding distance scales, so a kernel in feature space weights samples uniformly. Although continuous distances degrade in the suboptimal embedding space, the relative proximity of nodes remains robust, letting a thresholded densification extract the highest-confidence similarities. However, PPR, as a multi-hop topological diffusion process, is more robust to noise than a continuous feature-space kernel. In short, embeddings are more reliable for discrete edge creation, but too noisy for continuous weighting.

3.2 Densification to Address Local Bias

To address the above limitation, we propose densifying the graph before applying the kernel. The densification procedure consists of three stages: (i) automatic selection of a densification threshold guided by graph homophily, (ii) dimensionality reduction of node embeddings via PCA to concentrate the informative signal and decouple the correlated feature dimensions, and (iii) construction of an anisotropic Gaussian similarity kernel with adaptive bandwidths to add informative edges. Together, these steps expand the effective neighborhood used by the structural kernel while avoiding excessive noise or over-densification.

To achieve densification, we exploit the embedding similarities in the encoder embedding space using a Gaussian kernel. This kernel has two advantages: (i) unlike other similarity measures (e.g., cosine), it captures the non-linearity of the embeddings; and ii) the bandwidth controls the range of effect to adjust for local or global densification. To densify the graph, we construct a new adjacency matrix $\tilde{\mathbf{A}}$:

$$[\tilde{\mathbf{A}}]_{ij} = \begin{cases} 1 & \text{if } [\mathbf{A}]_{ij} = 1 \\ k_h(\mathbf{x}_i, \mathbf{x}_j) & \text{if } [\mathbf{A}]_{ij} = 0 \text{ and } k_h(\mathbf{x}_i, \mathbf{x}_j) \geq \tau_d \\ 0 & \text{o.w.} \end{cases} \quad (5)$$

where $k_h(\mathbf{x}_i, \mathbf{x}_j) = \frac{1}{(2\pi h^2)^{\frac{d_z}{2}}} \exp(-\frac{\|\mathbf{x}_i - \mathbf{x}_j\|_2^2}{2h^2})$ is the Gaussian kernel with bandwidth h , and τ_d is a similarity threshold for densification. Then, for the transition matrix of the PPR-based kernel, we have $\mathbf{M} = \tilde{\mathbf{D}}^{-1} \tilde{\mathbf{A}}$, where $\tilde{\mathbf{D}}$ is a diagonal matrix with $\tilde{\mathbf{D}}_{ii} = \sum_{j=1}^{|\mathcal{V}|} [\tilde{\mathbf{A}}]_{ij}$.

The densification threshold τ_d effectively determines the number of edges added. Small threshold values result in a nearly complete graph, increasing computational time. Moreover, the message-passing embeddings generated may be insufficiently discriminative; thus, smaller thresholds may allow the addition of potentially noisy edges. Conversely, large thresholds may hinder the addition of new edges, thereby missing informative edges that can overcome the sparsity barrier in applying the PPR-based kernel. Inspired by our empirical observations (Appendix A.3), we propose an automatic method to set the threshold in Appendix A.5. Note that the edge augmentation is applied uniformly to the entire graph before conformal weighting and sampling, independent of the train, calibration, or test split. Thus, the calibration–test symmetry required for conformal validity is preserved.

Dimensionality Reduction. Two pivotal issues with GNN embeddings are as follows: (i) dimensional information redundancy [38], i.e., feature dimensions are highly correlated, and (ii) the lack of discriminative power due to over-smoothing [35]. These accumulate noise and errors in similarity measures derived from the raw, high-dimensional, ill-posed space.

To address this, we use PCA [39] to decouple feature correlations and condense the embedding space. Formally, PCA solves the optimization problem $\mathbf{V}^{pca} = \arg \max_{\mathbf{V}} \mathbf{V}^T \mathbf{C}_X \mathbf{V}$, where $\mathbf{V} \in \mathbb{R}^{d_x \times d_z}$ is an orthogonal matrix. This yields the eigenvector matrix $\mathbf{V}^{pca} = [\mathbf{v}_1, \dots, \mathbf{v}_d]^T$ associated with the diagonal eigenvalue matrix $\mathbf{\Lambda}^{pca} = \text{diag}(\lambda_1, \lambda_2, \dots, \lambda_d)$, where eigenvalues are arranged in descending order, i.e., $\lambda_i \geq \lambda_j$ for all $i < j$. Here, $\mathbf{C}_X = \frac{1}{n} \mathbf{X}_{cal}^T \mathbf{X}_{cal}$ denotes the covariance matrix of the centered calibration data. To reduce dimensionality, we retain the eigenvectors corresponding to the c largest eigenvalues to construct $\mathbf{V}_c \in \mathbb{R}^{d_x \times c}$ and $\mathbf{\Lambda}_c \in \mathbb{R}^{c \times c}$. The transformed embeddings are then denoted as $\mathbf{z}_i = \mathbf{V}_c^T \mathbf{x}_i$. These embeddings serve as input to the Gaussian kernel for densification, as defined in Eq. 5. Selecting the top principal eigenvectors captures the directions of maximum variance and remedies the negative effect of over-smoothing, which diminishes high-frequency features faster than low-frequency features, reducing the separability of the embeddings [22].

Selecting Informative Edges by Adaptive Bandwidth. Even in the reduced space, samples are not uniformly distributed: topological bottlenecks often make embeddings dense in some directions and sparse in others. Proximity in such non-uniform distributions cannot be effectively captured by an isotropic Gaussian kernel, which assumes equal variance across all dimensions. In contrast, an anisotropic kernel accounts for varying scales across dimensions and captures geometric correlations. Therefore, we construct an anisotropic Gaussian kernel with adaptive bandwidth.

The PCA projection offers a specific advantage: the variance of the projected data along each principal component equals its corresponding eigenvalue. This motivates us to adaptively set the bandwidths of the anisotropic Gaussian kernel based on the PCA eigenvalues. Formally, our Gaussian kernel in

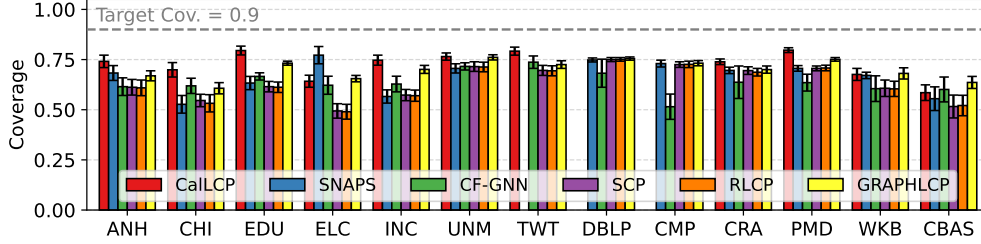


Figure 2: Results for WSC on regression and classification datasets. Miscoverage rate $\alpha = 0.1$. Our method generally outperforms the baselines on large classification datasets, while achieving second-best results on small regression datasets.

the PCA projection space is defined as:

$$H(\mathbf{x}, \mathbf{x}'; h^2 \mathbf{\Lambda}_c) = \exp\left(-\frac{1}{2} D_M^2(\mathbf{x}, \mathbf{x}'; h^2 \mathbf{\Lambda}_c)\right) \quad (6)$$

where $D_M^2(\mathbf{x}, \mathbf{x}'; h^2 \mathbf{\Lambda}_c) = (\mathbf{x} - \mathbf{x}')^T (h^2 \mathbf{\Lambda}_c)^{-1} (\mathbf{x} - \mathbf{x}')$ is the Mahalanobis distance, and h is a scalar base bandwidth. Once we apply PCA, we use \mathbf{z}_i instead of \mathbf{x}_i in Eq. 6.

Weighted Quantile Computation and Prediction. After graph densification, anchor point sampling, we apply the structure-aware weighting as in Eq. 4 and use the weights for computing the weighted quantile $\hat{q}_{1-\alpha}(\mathbf{x}_{n+1}, \tilde{\mathbf{x}}_{n+1})$ following Eq.1. Finally we derive the prediction set or interval as $\hat{C}_n^{\text{GRAPHLCP}}(\mathbf{x}_{n+1}, \tilde{\mathbf{x}}_{n+1}) = \{y \in \mathcal{Y} : s(\mathbf{x}_{n+1}, y) \leq \hat{q}_{1-\alpha}(\mathbf{x}_{n+1}, \tilde{\mathbf{x}}_{n+1})\}$.

GRAPHLCP builds on results showing that permutation-invariant GNN operations preserve exchangeability on graph data [18, 27], ensuring transductive conformal validity, while structural weighting improves relaxed conditional coverage.

Algorithm 1 in Appendix A.4 presents the pseudocode of our proposed method GRAPHLCP.

4 Experiments

Datasets. We show performance across *seven node regression* datasets, and *six node classification* datasets, and provide their details and statistics in the Appendix A.10.

Metrics. We show marginal coverage as a conventional metric. However, as discussed in Sec. 3, our localization-based approach is more advantageous for efficient relaxed conditional coverage. Therefore, for conditional CP, we use two settings from the recent comprehensive work on conditional CP diagnostics [4]. 1) Worst-case diagnostics: we evaluate worst-slab coverage (WSC) [34, 5]. 2) Group-based diagnostics: we show *four* feature-based groupings (partitioning).

Baselines. For validity, we compare with various baselines: vanilla split CP (SCP), two localized CP methods, namely RLCP [16] and CalLCP [14], and three graph-specific methods, specifically NAPS [7], CF-GNN[18], and SNAPS [40]. CalLCP’s high computational cost on large graphs exceeded our 3-day time limit, so it is occasionally excluded from our results. We fix the miscoverage rate to $\alpha = 0.1$ across all experiments. Additional details on other settings are provided in Appendix A.6.

4.1 Results on Conditional and Marginal CP

4.1.1 Conditional Coverage

We evaluate the conditional coverage under worst-case and group-based settings. Note that the worst-case setting using *WSC is the most challenging evaluation*, as it is an optimization-based evaluation that adversarially seeks a bounded interval along a projection direction where a sufficient number of test points exhibit the minimum coverage. Therefore, searching across a large number of directions could reveal the method’s lowest conditional coverage.

Worst-case Setting. We take 100 random direction vectors sampled uniformly from the unit sphere. The results are presented in Figure 2 for both classification and regression datasets. The results clearly show that GRAPHLCP with a structure-aware kernel can achieve the best or second-best results

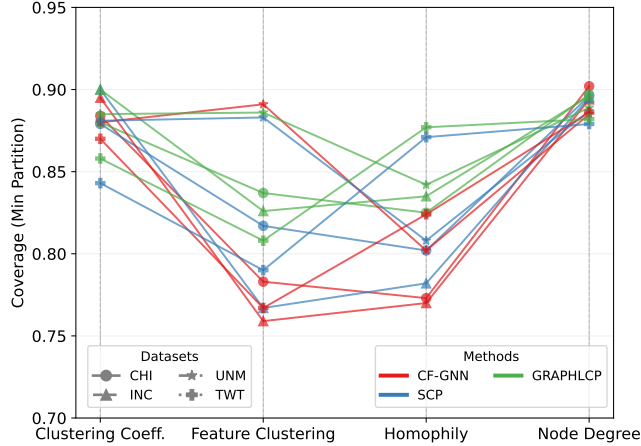


Figure 4: Results for group-based conditional coverage. It shows the minimum coverage across partitions for semantic and structural features where $\alpha = 0.1$. GRAPHLCP demonstrates superior coverage compared to baselines and more specifically in homophily and feature clustering.

by capturing node dependencies. Specifically, GRAPHLCP mostly outperforms the strong baseline CalLCP on classification datasets, while performing competitively with it on regression datasets. On larger graphs, the densification mechanism helps capture long-range semantic dependencies.

Next, we design an experiment to simultaneously compare validity and efficiency. Specifically, we collect worst-case coverage (WSC) and prediction length across datasets, and show in Figure 3, along with the method’s centroid of performance across all considered. The prediction lengths (sizes) are normalized by the maximum length across all methods. Although GRAPHLCP achieves the second-best WSC (coverage) sometimes in Figure 2; the results in Figure 3 suggest that GRAPHLCP performs better in terms of normalized prediction length than CalLCP, making the conformal sets more efficient.

Group-based Setting. Next, we evaluate group-based metrics, where we partition or group the test samples, based on different semantics, as of *Feature Clustering* based on the message-passing embeddings, and structural, as of *Clustering Coefficient*, *Homophily*, and *Node Degree*. This enables us to test the methods on the feature-stratified conditional coverage [4]. For each feature, we partition the data into three equal quantiles: “Low”, “Mid”, and “High”. We select four datasets that allow this 3-way partitioning, and bring the worst coverage across all partitions in Figure 4 for every feature. The general pattern shows the superiority of GRAPHLCP and is consistent with the results from the WSC experiments.

The effect of the two major components of GRAPHLCP becomes obvious from the group-based conditional coverage results, where we consistently outperform baselines. GRAPHLCP leverages structural information motivated by empirical evidence of homophily’s importance in graph-based CP (see Appendix A.3)). Also, our adaptive densification threshold is based on homophily. These lead to superior coverage of GRAPHLCP when the partitioning depends on homophily. In addition, when partitions are based on the feature clustering, GRAPHLCP outperforms the baselines.

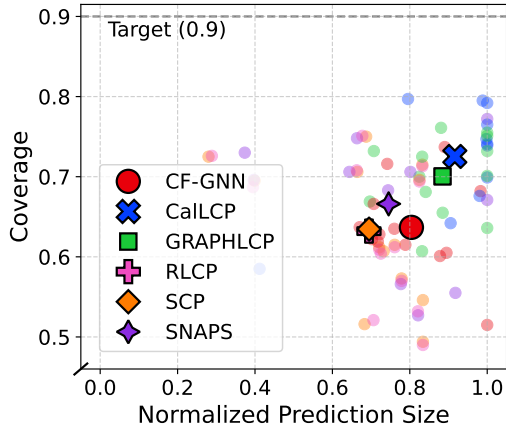


Figure 3: Results for WSC and efficiency on all datasets. While GRAPHLCP achieves the second-best WSC, it outperforms CalLCP in normalized prediction length.

Table 1: Marginal coverage results. All methods satisfy the target miscoverage of $\alpha = 0.1$. “-” means infinite-length prediction interval. OOT (out-of-time) takes an unreasonably long time.

Method	ANH	CHI	EDU	ELC	INC	UNM	TWT	CMP	CRA	DBLP	CBAS	WKB	PMD
CalLCP	0.939 \pm .01	0.939 \pm .01	0.937 \pm .00	0.936 \pm .01	0.936 \pm .00	0.937 \pm .00	0.942 \pm .00	OOT	0.907 \pm .01	OOT	0.943 \pm .01	0.933 \pm .01	0.917 \pm .00
SCP	0.902 \pm .01	0.904 \pm .01	0.905 \pm .01	0.902 \pm .01	0.903 \pm .00	0.905 \pm .01	0.902 \pm .01	0.901 \pm .00	0.902 \pm .00	0.900 \pm .00	0.898 \pm .01	0.898 \pm .02	0.900 \pm .00
NAPS	-	-	-	-	-	-	0.950 \pm .01	0.934 \pm .00	0.986 \pm .00	0.987 \pm .00	1.000 \pm .00	1.000 \pm .00	0.990 \pm .00
CF-GNN	0.920 \pm .01	0.911 \pm .01	0.901 \pm .01	0.898 \pm .01	0.900 \pm .01	0.900 \pm .01	0.908 \pm .01	0.902 \pm .00	0.905 \pm .01	0.900 \pm .00	0.915 \pm .02	0.900 \pm .02	0.901 \pm .00
SNAPS	0.923 \pm .01	0.899 \pm .01	0.916 \pm .01	0.969 \pm .01	0.903 \pm .01	0.896 \pm .01	-	0.901 \pm .00	0.902 \pm .00	0.900 \pm .00	0.896 \pm .02	0.898 \pm .01	0.900 \pm .00
RLCP	0.900 \pm .01	0.900 \pm .01	0.903 \pm .01	0.900 \pm .01	0.901 \pm .00	0.904 \pm .01	0.900 \pm .01	0.901 \pm .00	0.900 \pm .00	0.900 \pm .00	0.897 \pm .01	0.895 \pm .02	0.900 \pm .00
GRAPHLCP	0.905 \pm .01	0.904 \pm .01	0.904 \pm .00	0.902 \pm .00	0.902 \pm .00	0.897 \pm .00	0.903 \pm .01	0.901 \pm .00	0.903 \pm .01	0.904 \pm .00	0.917 \pm .01	0.903 \pm .01	0.904 \pm .00

Table 2: Isolated kernel type effect. Generally, a PPR kernel provides both better coverage and a tighter prediction interval/set than a Gaussian (GSS) kernel.

Measure	Variant	ANH	CHI	EDU	ELC	INC	UNM	TWT	CRA	CBAS	WKB
Coverage	GSS	0.63 \pm .05	0.58 \pm .03	0.69 \pm .02	0.54 \pm .03	0.66 \pm .02	0.72 \pm .02	0.71 \pm .03	0.69 \pm .02	0.52 \pm .06	0.68 \pm .02
	PPR	0.67 \pm .03	0.60 \pm .03	0.71 \pm .01	0.62 \pm .02	0.69 \pm .02	0.76 \pm .01	0.71 \pm .02	0.72 \pm .01	0.64 \pm .03	0.63 \pm .03
Pred. Len.	GSS	1.66 \pm .12	1.95 \pm .06	2.25 \pm .14	1.04 \pm .03	2.14 \pm .10	1.79 \pm .05	2.09 \pm .13	0.93 \pm .04	2.04 \pm .10	4.01 \pm .10
	PPR	1.61 \pm .08	1.93 \pm .04	2.10 \pm .13	1.01 \pm .03	1.99 \pm .08	1.78 \pm .03	2.10 \pm .12	2.81 \pm .02	2.91 \pm .11	3.43 \pm .12

4.1.2 Marginal Coverage

Evaluating marginal coverage is a sanity check for a CP method. Results in Table 1 show that all methods achieve a miscoverage rate $\alpha = 0.1$, showing the insufficiency of this metric for evaluation. We present marginal prediction length results in the Appendix A.8.

4.2 Ablation Studies

PPR Kernel vs. Gaussian Kernel. Our method achieves robust conditional coverage by replacing standard embedding-space proximity with a structure-aware PPR kernel. To isolate the effect of structural localization from that of reconditioning the embedding space during densification, we replace our structural PPR weighting with an Gaussian kernel (GSS) applied directly to the PCA-transformed embeddings, keeping the densification and adaptive bandwidth unchanged. The results in Table 2 show that the PPR kernel provides a clear independent benefit, as it simultaneously increases WSC and yields tighter Prediction Length (PL). These results support our main claim that structure-aware localization is the key component.

Add-on Effects. While GRAPHLCP relies heavily on the structure due to the PPR-based kernel, the densification step, which implicitly incorporates useful information from the embedding space, plays an important role. We ablate individual components of our model to evaluate their specific contributions, as summarized in Table 3. WSC is an optimization-based adversarial metric. This makes absolute numerical improvements bounded and small, while they can represent high relative gains over baselines. Therefore, we also report %NI, which denotes the percentage of improvement normalized by the maximum coverage difference across all methods. First, the densification step often has the largest effect, particularly on regression datasets (ANH, CHI, and TWT). The next most significant contributor is the PCA projection, which shows the importance of avoiding the negative effects of correlated embedding features to remedy over-smoothing and to condense the embedding space. Although dynamic bandwidth makes a lesser contribution, it is advantageous in controlling the number of augmented edges, which can significantly reduce the computational time of the densification step and PPR weight computation.

5 Conclusion

We have introduced GRAPHLCP, a structure-aware localized conformal prediction framework for GNNs that explicitly incorporates graph topology into conformal localization and weighting. By replacing embedding-only proximity with a Personalized PageRank-based kernel, our method achieves reliable marginal coverage while improving efficiency and relaxed test-conditional behavior. With experiments on multiple regression and classification datasets, GRAPHLCP demonstrate consistently produces better localized prediction sets than existing graph conformal baselines. We believe this

Table 3: Ablation study on the main components across regression and classification with $\alpha = 0.1$. Results show that the most significant component is densification particularly for regression.

Variant	ANH			CHI			EDU			UNM			CBAS			WKB			TWT		
	Cov	%NI	Size	Cov	%NI	Size	Cov	%NI	Size	Cov	%NI	Size	Cov	%NI	Size	Cov	%NI	Size	Cov	%NI	Size
GRAPHLCP	0.67 \pm .03	-	1.61 \pm .09	0.61 \pm .03	-	1.94 \pm .03	0.73 \pm .01	-	2.66 \pm .26	0.76 \pm .01	-	1.91 \pm .13	0.64 \pm .03	-	2.91 \pm .11	0.68 \pm .03	-	3.55 \pm .14	0.72 \pm .02	-	2.11 \pm .15
w/o Densification	0.51 \pm .02	123.1	1.36 \pm .09	0.51 \pm .03	58.8	1.85 \pm .05	0.71 \pm .01	10.5	2.87 \pm .54	0.73 \pm .01	50.0	1.93 \pm .13	0.65 \pm .02	-12.5	3.00 \pm .08	0.62 \pm .04	75.0	3.36 \pm .14	0.67 \pm .02	38.5	2.09 \pm .10
w/o PCA	0.66 \pm .03	7.7	1.61 \pm .06	0.59 \pm .03	11.8	1.93 \pm .04	0.71 \pm .02	10.5	2.10 \pm .14	0.76 \pm .01	0.0	1.79 \pm .03	0.64 \pm .03	0.0	2.91 \pm .11	0.60 \pm .02	100.0	3.49 \pm .13	0.72 \pm .02	0.0	2.10 \pm .12
w/o Dynamic h	0.67 \pm .03	0.0	1.61 \pm .08	0.60 \pm .03	5.9	1.93 \pm .04	0.71 \pm .01	10.5	2.10 \pm .13	0.76 \pm .01	0.0	1.78 \pm .03	0.64 \pm .03	0.0	2.91 \pm .11	0.63 \pm .03	62.5	3.43 \pm .12	0.71 \pm .02	7.7	2.10 \pm .12

work highlights the importance of structure-aware localization for UQ on graphs. An important future direction is to extend localized conformal prediction to dynamic graphs with evolving topologies.

References

- [1] Anastasios N Angelopoulos and Stephen Bates. A gentle introduction to conformal prediction and distribution-free uncertainty quantification. *arXiv preprint arXiv:2107.07511*, 2021.
- [2] Rina Foygel Barber, Emmanuel J. Candès, Aaditya Ramdas, and Ryan J. Tibshirani. Conformal prediction beyond exchangeability. *The Annals of Statistics*, 2022.
- [3] Aleksandar Bojchevski and Stephan Günnemann. Deep gaussian embedding of graphs: Unsupervised inductive learning via ranking. In *International Conference on Learning Representations*, 2018.
- [4] Sacha Braun, David Holzmüller, Michael I. Jordan, and Francis Bach. Conditional coverage diagnostics for conformal prediction, 2025.
- [5] Maxime Cauchois, Suyash Gupta, and John C. Duchi. Knowing what you know: valid and validated confidence sets in multiclass and multilabel prediction. *J. Mach. Learn. Res.*, 22(1), January 2021.
- [6] Dawei Cheng, Yao Zou, Sheng Xiang, and Changjun Jiang. Graph neural networks for financial fraud detection: a review. *Frontiers of Computer Science*, 19(9):199609, 2025.
- [7] Jase Clarkson. Distribution free prediction sets for node classification. In *Proceedings of the 40th International Conference on Machine Learning, ICML’23*. JMLR.org, 2023.
- [8] Evan N Feinberg, Harsh Suratia, and Amir Saffari. Potentialnet for molecular property prediction. *Journal of chemical information and modeling*, 58(6):1194–1201, 2018.
- [9] Rina Foygel Barber, Emmanuel J Candès, Aaditya Ramdas, and Ryan J Tibshirani. The limits of distribution-free conditional predictive inference. *Information and Inference: A Journal of the IMA*, 10(2):455–482, 08 2020.
- [10] Johannes Gasteiger, Aleksandar Bojchevski, and Stephan Günnemann. Combining neural networks with personalized pagerank for classification on graphs. In *International Conference on Learning Representations*, 2019.
- [11] Justin Gilmer, Samuel S. Schoenholz, Patrick F. Riley, Oriol Vinyals, and George E. Dahl. Neural message passing for quantum chemistry. In *Proceedings of the 34th International Conference on Machine Learning - Volume 70, ICML’17*, page 1263–1272. JMLR.org, 2017.
- [12] Francesco Di Giovanni, T. Konstantin Rusch, Michael Bronstein, Andreea Deac, Marc Lackenby, Sidhartha Mishra, and Petar Veličković. How does over-squashing affect the power of GNNs? *Transactions on Machine Learning Research*, 2024.
- [13] Jhony H. Giraldo, Konstantinos Skianis, Thierry Bouwmans, and Fragkiskos D. Malliaros. On the trade-off between over-smoothing and over-squashing in deep graph neural networks. In *Proceedings of the 32nd ACM International Conference on Information and Knowledge Management, CIKM ’23*, page 566–576, New York, NY, USA, 2023. Association for Computing Machinery.
- [14] Laying Guan. Localized conformal prediction: a generalized inference framework for conformal prediction. *Biometrika*, 110(1):33–50, 07 2022.
- [15] Shurui Gui, Xiner Li, Limei Wang, and Shuiwang Ji. GOOD: A graph out-of-distribution benchmark. In *Thirty-sixth Conference on Neural Information Processing Systems Datasets and Benchmarks Track*, 2022.
- [16] Rohan Hore and Rina Foygel Barber. Conformal prediction with local weights: randomization enables robust guarantees. *Journal of the Royal Statistical Society Series B: Statistical Methodology*, 87(2):549–578, 11 2024.

- [17] Hans Hao-Hsun Hsu, Yuesong Shen, Christian Tomani, and Daniel Cremers. What makes graph neural networks miscalibrated? In S. Koyejo, S. Mohamed, A. Agarwal, D. Belgrave, K. Cho, and A. Oh, editors, *Advances in Neural Information Processing Systems*, volume 35, pages 13775–13786. Curran Associates, Inc., 2022.
- [18] Kexin Huang, Ying Jin, Emmanuel Candes, and Jure Leskovec. Uncertainty quantification over graph with conformalized graph neural networks. *NeurIPS*, 2023.
- [19] Glen Jeh and Jennifer Widom. Scaling personalized web search. In *Proceedings of the 12th International Conference on World Wide Web, WWW '03*, page 271–279, New York, NY, USA, 2003. Association for Computing Machinery.
- [20] Junteng Jia and Austion R. Benson. Residual correlation in graph neural network regression. In *Proceedings of the 26th ACM SIGKDD International Conference on Knowledge Discovery & Data Mining, KDD '20*, page 588–598, New York, NY, USA, 2020. Association for Computing Machinery.
- [21] Sunay Joshi, Shayan Kiyani, George J. Pappas, Edgar Dobriban, and Hamed Hassani. Conformal inference under high-dimensional covariate shifts via likelihood-ratio regularization. In *The Thirty-ninth Annual Conference on Neural Information Processing Systems*, 2025.
- [22] Nicolas Keriven. Not too little, not too much: a theoretical analysis of graph (over)smoothing. In *Proceedings of the 36th International Conference on Neural Information Processing Systems, NIPS '22*, Red Hook, NY, USA, 2022. Curran Associates Inc.
- [23] Thomas N. Kipf and Max Welling. Semi-supervised classification with graph convolutional networks. In *International Conference on Learning Representations*, 2017.
- [24] Arun Kumar Kuchibhotla. Exchangeability, conformal prediction, and rank tests, 2021.
- [25] Siddhartha Laghuvarapu, Zhen Lin, and Jimeng Sun. Codrug: conformal drug property prediction with density estimation under covariate shift. In *Proceedings of the 37th International Conference on Neural Information Processing Systems, NIPS '23*, Red Hook, NY, USA, 2023. Curran Associates Inc.
- [26] Xixun Lin, Yanan Cao, Nan Sun, Lixin Zou, Chuan Zhou, Peng Zhang, Shuai Zhang, Ge Zhang, and Jia Wu. Conformal graph-level out-of-distribution detection with adaptive data augmentation. In *Proceedings of the ACM on Web Conference 2025, WWW '25*, page 4755–4765, New York, NY, USA, 2025. Association for Computing Machinery.
- [27] Robert Lunde. On the validity of conformal prediction for network data under non-uniform sampling, 2023.
- [28] Robert Lunde, Elizaveta Levina, and Ji Zhu. Conformal prediction for network-assisted regression. *Journal of the American Statistical Association*, 120(551):1633–1644, 2025.
- [29] Minbo Ma, Peng Xie, Fei Teng, Bin Wang, Shenggong Ji, Junbo Zhang, and Tianrui Li. Histgmn: Hierarchical spatio-temporal graph neural network for weather forecasting. *Information Sciences*, 648:119580, 2023.
- [30] Ariane Marandon. Conformal link prediction for false discovery rate control. *TEST*, 33:1062 – 1083, 2023.
- [31] Huda Nassar, Kyle Kloster, and David F. Gleich. Strong localization in personalized pagerank vectors. In *Proceedings of the 12th International Workshop on Algorithms and Models for the Web Graph - Volume 9479, WAW 2015*, page 190–202, Berlin, Heidelberg, 2015. Springer-Verlag.
- [32] Athanasios N. Nikolakopoulos, Xia Ning, Christian Desrosiers, and George Karypis. Trust your neighbors: A comprehensive survey of neighborhood-based methods for recommender systems. *ArXiv*, abs/2109.04584, 2021.
- [33] Oyebade K. Oyedotun, Kassem Al Ismaeil, and Djamila Aouada. Why is everyone training very deep neural network with skip connections? *IEEE Transactions on Neural Networks and Learning Systems*, 34(9):5961–5975, 2023.
- [34] Yaniv Romano, Matteo Sesia, and Emmanuel J. Candès. Classification with valid and adaptive coverage. In *Proceedings of the 34th International Conference on Neural Information Processing Systems, NIPS '20*, Red Hook, NY, USA, 2020. Curran Associates Inc.
- [35] T. Konstantin Rusch, Michael M. Bronstein, and Siddhartha Mishra. A survey on oversmoothing in graph neural networks, 2023.

- [36] Glenn Shafer and Vladimir Vovk. A tutorial on conformal prediction. *Journal of Machine Learning Research*, 9(3), 2008.
- [37] Oleksandr Shchur, Maximilian Mumme, Aleksandar Bojchevski, and Stephan Günnemann. Pitfalls of graph neural network evaluation, 2019.
- [38] Wei Shen, Mang Ye, and Wenke Huang. Resisting over-smoothing in graph neural networks via dual-dimensional decoupling. In *ACM Multimedia 2024*, 2024.
- [39] Jonathon Shlens. A tutorial on principal component analysis, 2014.
- [40] Jianqing Song, Jianguo Huang, Wenyu Jiang, Baoming Zhang, Shuangjie Li, and Chongjun Wang. Similarity-navigated conformal prediction for graph neural networks. In *The Thirty-eighth Annual Conference on Neural Information Processing Systems*, 2024.
- [41] Ryan J Tibshirani, Rina Foygel Barber, Emmanuel Candes, and Aaditya Ramdas. Conformal prediction under covariate shift. In H. Wallach, H. Larochelle, A. Beygelzimer, F. d'Alché-Buc, E. Fox, and R. Garnett, editors, *Advances in Neural Information Processing Systems*, volume 32. Curran Associates, Inc., 2019.
- [42] Vladimir Vovk, Alex Gammerman, and Glenn Shafer. *Algorithmic Learning in a Random World*. Springer, 2005. Springer, New York.
- [43] Xiao Wang, Hongrui Liu, Chuan Shi, and Cheng Yang. Be confident! towards trustworthy graph neural networks via confidence calibration. In A. Beygelzimer, Y. Dauphin, P. Liang, and J. Wortman Vaughan, editors, *Advances in Neural Information Processing Systems*, 2021.
- [44] Soroush H Zargarbashi, Simone Antonelli, and Aleksandar Bojchevski. Conformal prediction sets for graph neural networks. In *International Conference on Machine Learning*, pages 12292–12318. PMLR, 2023.
- [45] Soroush H. Zargarbashi and Aleksandar Bojchevski. Conformal inductive graph neural networks. In *The Twelfth International Conference on Learning Representations*, 2024.
- [46] Zheng Zhang, Jie Bao, Zhixin Zhou, Nicolo Colombo, Lixin Cheng, and Rui Luo. Residual reweighted conformal prediction for graph neural networks. In *Proceedings of the Forty-First Conference on Uncertainty in Artificial Intelligence, UAI '25. JMLR.org*, 2025.
- [47] Tianyi Zhao, Jian Kang, and Lu Cheng. Conformalized link prediction on graph neural networks. In *Proceedings of the 30th ACM SIGKDD Conference on Knowledge Discovery and Data Mining, KDD '24*, page 4490–4499, New York, NY, USA, 2024. Association for Computing Machinery.

A Appendix

A.1 Additional Related Work

Conformal Prediction (CP), Weighted CP (WCP), and Localized CP (LCP) Unlike single-point predictors that do not quantify uncertainty [36], CP provides a simple distribution-free framework for constructing prediction sets in classification and prediction intervals in regression with finite-sample guarantees [36, 1, 42]. CP’s validity comes from the assumption of exchangeability, and as a distribution-free method, it does not rely on strong parametric assumptions or strict distributions. [24, 42]. The high variance in marginal coverage across different regions of the data distribution has increased interest in conditional CP although exact conditional coverage cannot generally be achieved in finite samples [9].

Many recent works study approximate or relaxed conditional coverage to improve coverage in heterogeneous settings by adapting prediction set sizes to the difficulty of individual instances [5, 34]. Also, several weighted CP methods have proposed relaxing standard exchangeability assumptions [41, 2]. These approaches typically estimate distribution ratios between calibration and test samples and use them to compute weighted quantiles [16, 14].

Similarly, localized CP (LCP) gives larger weights to calibration points that are more similar to the test instance to improve local coverage behavior [41, 16]. From this category, Randomized LCP (RLCP) further introduces randomization and anchor sampling strategies to improve coverage around the test point itself rather than only its surrounding neighborhood [16]. Still, most localized methods depend heavily on the quality of the feature representation used to measure similarity [21, 16]. In high-dimensional settings or when embeddings are poorly structured, defining reliable local neighborhoods becomes difficult and can lead to inefficient prediction intervals [2, 21].

Uncertainty Quantification in Graph Neural Networks (GNNs) Calibration remains a challenge in graph neural networks (GNNs) since 1) their learned representations are often not sufficiently separable or reliable [43, 17], and 2) predictions are not uniformly reliable across different regions of the graph due to structural effects [7, 17]. This is particularly important in high-stakes applications such as drug discovery or fraud detection, where inaccurate confidence estimates may lead to unreliable decisions [8, 6, 17]. In addition, under heterophily, GNNs can suffer from over-squashing, while deeper architectures are also prone to over-smoothing [13, 35]. As a result, node embeddings may become noisy or less informative for measuring similarity, which limits the application of existing LCP methods to graph data as they rely heavily on stable embedding-space distances [13, 16].

Conformal Prediction on Graphs Applying CP to graph data is challenging because node dependencies violate the standard i.i.d. assumption [27, 7]. Still, prior work has shown that exchangeability can hold in transductive settings for conventional GNNs due to permutation invariance, which supports the use of finite-sample CP guarantees on graph data [24, 18, 27]. This has motivated CP for graph tasks such as link prediction and out-of-distribution detection [26, 30, 47].

Recent graph CP methods often incorporate additional structural or contextual information during calibration [7, 18, 46]. Some approaches use embedding-space density estimates for weighting [25], while others rely on structural partitioning [46], graph diffusion scores [44], or combinations of node features and graph topology to adapt nonconformity scores [40]. Many of these methods remain sensitive to embedding quality or rigid graph partitions. Our approach instead uses a structure-aware kernel to improve localization when feature-space similarity is unreliable.

A.2 Limitations of RLCP

While RLCP excels in low-dimensional settings, its application to GNNs is hindered by poor embedding discriminability. GNN embeddings often exhibit high feature correlation, non-uniformity, and over-smoothing. Consequently, applying a Gaussian kernel here tends to collapse the distribution toward a Dirac delta or a uniform weight. We verify this behavior by measuring the weights of the calibration and test samples across varying bandwidths.

Figure 5 shows the empirical cumulative distribution function (ECDF) for calibration (dashed) and test (solid) weights according to sampled anchor points for a Gaussian kernel applied in the embedding space for different bandwidths. Small bandwidth assigns almost all the weight to the

test points (i.e., $w_{n+1} \simeq 1.0$), leaving the calibration nodes with identical weights close to zero, i.e., $w_i \simeq 0.0 : \forall i \in [n]$. This pushes the estimated quantile $\hat{q}_{1-\alpha}(\mathbf{x}_{n+1}, \tilde{\mathbf{x}}_{n+1}) \simeq +\infty$ to infinity according to Eq. 1. Whereas, larger bandwidths yield identical weights for all points due to indiscriminate, over-smoothed embeddings. This reduces RLCP to standard SCP, ignoring local proximity for better test conditional coverage. We address this by introducing GRAPHLCP, which explicitly incorporates graph-structural proximity.

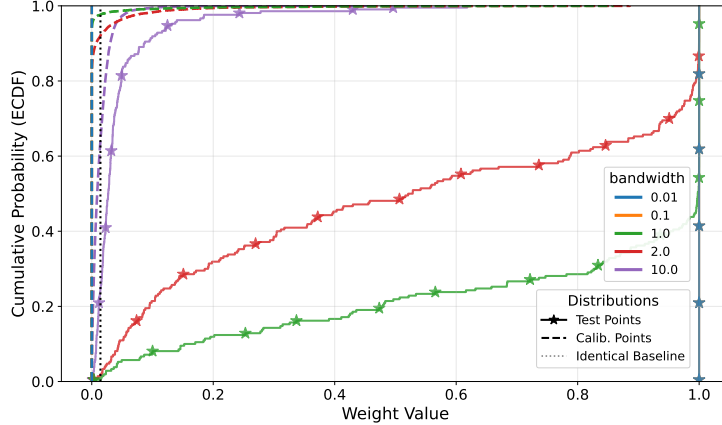


Figure 5: GOODCBAS dataset: Impact of Gaussian kernel bandwidth h on RLCP weight distribution. Low bandwidths concentrate probability mass on test points, leaving calibration points with near-zero weights. Conversely, large bandwidths cause weights to jump toward a uniform distribution where all points receive near-zero values.

A.3 Empirical Insights and Design Principle

Our assumption is that weighted CP can highly benefit from nodes’ structural dependencies. We confirm this assumption by an experiment that shows the effect of node homophily on the coverage and prediction length of vanilla SCP (defined in Sec. 2.2). For classification datasets, a node’s homophily ratio $\eta_u = \frac{|\{v \in \mathcal{N}_u : y_v = y_u\}|}{|\mathcal{N}_u|}$ and for regression datasets, we have $\eta_u = 1 - \frac{1}{|\mathcal{N}_u|} \sum_{v \in \mathcal{N}_u} \frac{|y_v - y_u|}{\max_{i,j: A_{ij}=1} |y_i - y_j|}$,

where y_u is target value (e.g. label) of u . Figure 6 elaborates on a common pattern: nodes with low homophily suffer from significant under-coverage, while high-homophily nodes are well covered, exhibiting an easier task. Also, the prediction lengths are generally stable or decrease with higher homophily ratios. This demonstrates that SCP fails to guarantee coverage for heterophilous nodes, even with a higher uncertainty budget.

Because uncertainty and graph topology are strongly correlated, we explicitly incorporate the underlying structure into our quantile weighting. GRAPHLCP replaces embedding-based kernels with a structure-aware kernel that governs both anchor sampling and weighting. By defining proximity through topology, we enable localized CP that respects structural dependencies and bypasses the suboptimality of message-passing embeddings [33]. GRAPHLCP comprises three components: (1) a Personalized PageRank-based localization kernel, (2) randomized anchor sampling and weighting compatible with RLCP, and (3) a feature-aware densification step to mitigate sparsity. These are detailed below.

A.4 Pseudocode for Our Method

Algorithm 1 presents the Pseudocode of the three main stages of our proposed method GRAPHLCP: 1) *graph densification* with a prior PCA projection and dynamic bandwidth setting step, 2) *anchor point sampling* according to a geometric distribution of random walk lengths, and 3) *weighting and quantile computation* using our structural-aware kernel.

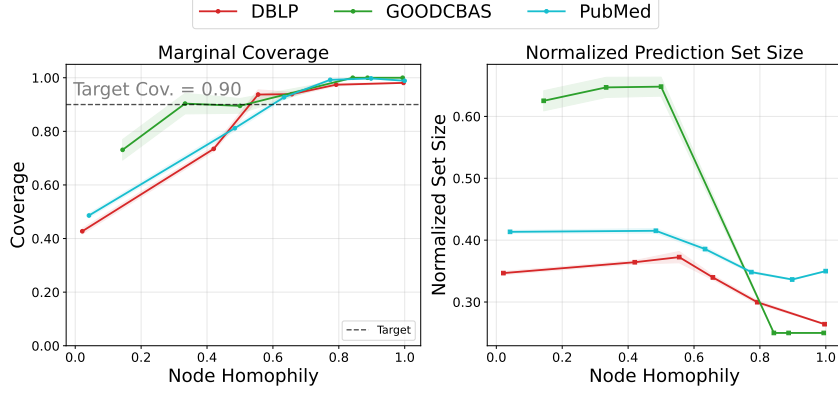


Figure 6: Impact of node homophily on the marginal coverage and prediction length/size of SCP. Satisfying coverage for more homophilous nodes is easier at the same or lower prediction length, underlining the significant contribution of graph structure in CP application for GNNs.

Algorithm 1 GRAPHLCP

- 1: **Input:** Graph $\mathcal{G} = (\mathcal{V}, \mathbf{A}, \mathbf{X})$, Calibration \mathcal{D}_{cal} , Test u_{n+1} , Params $\alpha, \alpha_{ppr}, c, h, \tau_d^*$
 - 2: **Output:** Prediction set $\hat{C}_n(\mathbf{x}_{n+1})$
 - 3: **Stage 1: Feature-Aware Densification**
 - 4: Compute graph homophily $\eta_{\mathcal{G}}$
 - 5: Optimize τ_d s.t. edge density $\rho \in \text{Bounds}(\eta_{\mathcal{G}}, \tau_d^*)$
 - 6: $\mathbf{V}_c, \mathbf{\Lambda}_c \leftarrow \text{PCA}(\mathbf{X}_{cal}, \text{top-}c)$
 - 7: **for** each pair (i, j) with $\mathbf{A}_{ij} = 0$ **do**
 - 8: $\mathbf{z}_i = \mathbf{V}_c^T \mathbf{x}_i; \mathbf{z}_j = \mathbf{V}_c^T \mathbf{x}_j$
 - 9: $s_{ij} \leftarrow \exp\left(-\frac{1}{2}(\mathbf{z}_i - \mathbf{z}_j)^T (h^2 \mathbf{\Lambda}_c)^{-1} (\mathbf{z}_i - \mathbf{z}_j)\right)$
 - 10: **if** $s_{ij} \geq \tau_d$ **then**
 - 11: $\hat{\mathbf{A}}_{ij} \leftarrow s_{ij}$
 - 12: **end if**
 - 13: **end for**
 - 14: **Stage 2: Anchor Sampling**
 - 15: $\mathbf{M} \leftarrow \hat{\mathbf{D}}^{-1} \hat{\mathbf{A}}$
 - 16: Sample walk length $k \sim \text{Geom}(\alpha_{ppr})$
 - 17: Sample \tilde{u}_{n+1} via k -step random walk from u_{n+1}
 - 18: **Stage 3: Weighting & Quantile Computation**
 - 19: Compute PPR vector $\tilde{\pi}_{n+1}$ seeded at anchor \tilde{u}_{n+1}
 - 20: **for** $i \in \mathcal{D}_{cal} \cup \{u_{n+1}\}$ **do**
 - 21: $\tilde{w}_i \leftarrow [\tilde{\pi}_{n+1}]_i / d_i$ {Symmetry correction}
 - 22: **end for**
 - 23: Normalize weights $\tilde{w}_i \leftarrow \tilde{w}_i / \sum \tilde{w}_j$
 - 24: $\hat{q} \leftarrow \text{Quantile}_{1-\alpha}\left(\sum \tilde{w}_i \delta_{s(\mathbf{x}_i, y_i)} + \tilde{w}_{n+1} \delta_{\infty}\right)$
 - 25: **return** $\{y \in \mathcal{Y} \mid s(\mathbf{x}_{n+1}, y) \leq \hat{q}\}$
-

A.5 Automatic Densification Threshold Setup.

Figure 6 shows that the homophily ratio highly impacts the uncertainty of the model. Therefore, the densification threshold can be set for all nodes of a graph according to the graph homophily ratio $\eta_{\mathcal{G}}$. Formally, starting with a threshold $\tau^{(0)} = \tau_d^*$, we adjust for T iterations as follows:

$$\tau^{(t+1)} = \begin{cases} \tau^{(t)} & t \geq T \text{ or } \rho_{\min} \leq \rho \leq \rho_{\max} \\ (1 - \gamma)\tau^{(t)} & \rho \leq \rho_{\min} \\ (1 + \gamma)\tau^{(t)} & \rho \geq \rho_{\max} \end{cases}$$

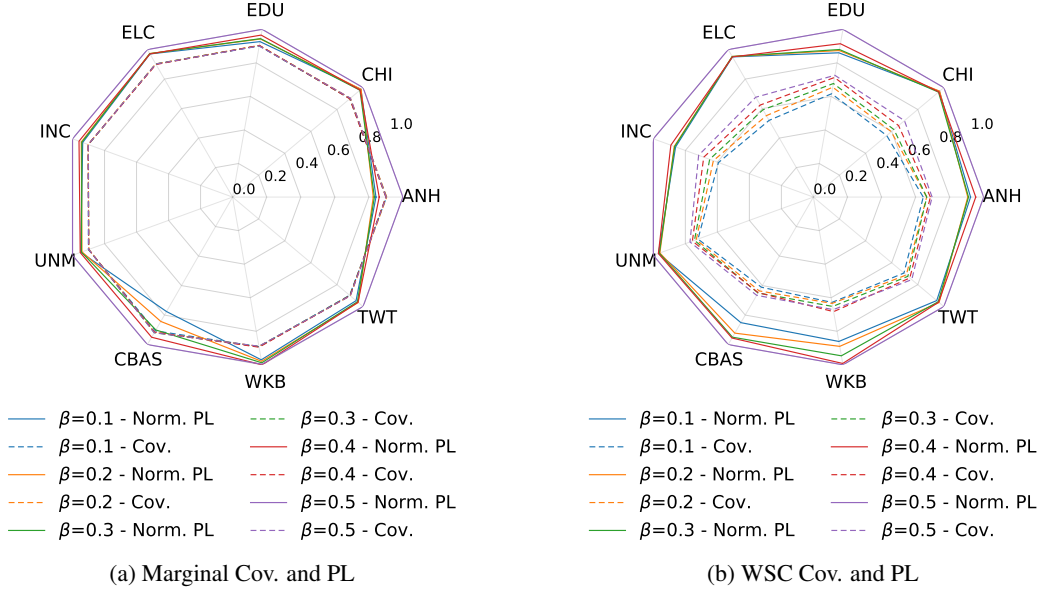


Figure 7: Sensitivity analysis of the PPR restart probability β . Higher β values prioritize local neighborhood information, leading to improved marginal and WSC coverage at the cost of a moderate increase in WSC PL.

where $\rho = \frac{\|\tilde{\mathbf{A}}\|_1}{\|\mathbf{A}\|_1}$ is the new edge ratio, s.t. $\|\tilde{\mathbf{A}}\|_1 = \sum_{i,j} [\tilde{\mathbf{A}}]_{ij}$ and $\|\mathbf{A}\|_1 = \sum_{i,j} [\mathbf{A}]_{ij}$. Also, $\rho_{\min} = 1 + \min(\eta_{\mathcal{G}}, (1 - \tau^{(0)}) * 2)$, and $\rho_{\max} = (1 - \eta_{\mathcal{G}})^{-1}$. Also, γ is a scaling factor (set to 0.1 in our experiments).

Unlike the densification threshold, which strictly controls the width of the context (embedding-based neighborhood) for each node to be considered, the bandwidth of the Gaussian kernel, more importantly, provides smooth control over local-to-global context. However, adjusting for an appropriate bandwidth is difficult, as shown in Figure 5.

A.6 Experimental Settings

For all datasets, we split each dataset into 4 sets: training, validation, calibration, and test. We train the models on the training set and use the validation set to tune the hyperparameters. Once the models are trained, we fix the pretrained models. The selection fractions (train, validation, calibration, test) are as follows: ANH, CHI, TWT: (0.4, 0.1, 0.1, 0.4) - CMP, CRA, DBLP, PMD, : (0.2, 0.1, 0.2, 0.5) - EDU, ELC, INC, UNM: (0.4, 0.1, 0.1, 0.4) - CBAS, WKB: (0.5, 0.1, 0.1, 0.3). We use GCN [23], as our pretrained model. Across all the experiments, we fix: miscoverage $\alpha = 0.1$, the number of APPNP steps, $K = 30$, the base bandwidth $h = 2.0$, the base densification threshold $\tau_d^* = 0.5$. We set β in (0.2, 0.4), and c for PCA between (5, 10). We run the experiments on a single GPU core NVIDIA GeForce RTX 3090 and x86_64 CPUs.

A.7 Additional Ablation Studies

The previous ablation studies clarified the significant impact of the PPR kernel and the densification step. Therefore, here analyze the effect of the two main hyperparameters within the setup of the PPR kernel and the densification.

PPR restart probability (β) First, we conduct a sensitivity analysis over the PPR restart probability $\beta \in [0.1, 0.5]$. This hyperparameter controls the kernel’s locality extent: lower values allow longer random walks, allowing more nodes to contribute to the weighted CP and vice versa. The results in Figure 7 show that increasing β improves both marginal and WSC (coverage) while moderately increasing PL (prediction length) of the worst-slab scenario. In other words, smaller β yields overly

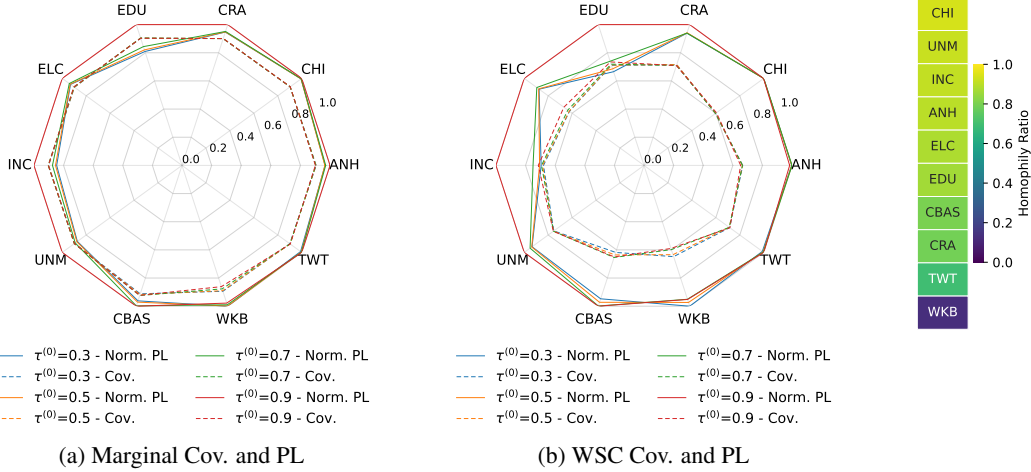


Figure 8: Sensitivity analysis of initial densification threshold $\tau_d^{(0)}$. There is a trade-off between edge noise and topological enhancement, with optimal coverage achieved by adapting the threshold to the dataset’s homophily level.

Table 4: WSC results. GRAPHLCP generally provides the second-best WSC coverage across all datasets. “-” means infinite-length prediction interval. OOT (out-of-time) shows results attained after an unreasonably long time.

Method	ANH	CHI	EDU	ELC	INC	UNM	TWT	CMP	CRA	DBLP	CBAS	WKB	PMD
CalLCP	0.74 \pm .03	0.70 \pm .04	0.80 \pm .02	0.64 \pm .03	0.75 \pm .03	0.77 \pm .02	0.79 \pm .02	OOT	0.74 \pm .01	OOT	0.58 \pm .04	0.68 \pm .03	0.80 \pm .01
SCP	0.61 \pm .04	0.55 \pm .03	0.61 \pm .03	0.49 \pm .04	0.57 \pm .03	0.71 \pm .02	0.70 \pm .03	0.72 \pm .01	0.69 \pm .02	0.75 \pm .01	0.52 \pm .06	0.61 \pm .04	0.71 \pm .01
NAPS	-	-	-	-	-	-	0.82 \pm .02	0.82 \pm .01	0.94 \pm .01	0.96 \pm .00	1.00 \pm .00	1.00 \pm .00	0.97 \pm .00
CF-GNN	0.61 \pm .04	0.62 \pm .04	0.67 \pm .02	0.62 \pm .04	0.63 \pm .04	0.72 \pm .02	0.74 \pm .03	0.52 \pm .06	0.64 \pm .08	0.68 \pm .07	0.60 \pm .06	0.60 \pm .06	0.64 \pm .04
SNAPS	0.68 \pm .04	0.53 \pm .04	0.63 \pm .03	0.77 \pm .04	0.57 \pm .03	0.71 \pm .02	-	0.73 \pm .02	0.70 \pm .02	0.75 \pm .01	0.56 \pm .06	0.67 \pm .02	0.71 \pm .01
RLCP	0.61 \pm .04	0.53 \pm .04	0.61 \pm .03	0.49 \pm .04	0.57 \pm .03	0.71 \pm .02	0.69 \pm .03	0.73 \pm .02	0.69 \pm .02	0.75 \pm .01	0.52 \pm .05	0.60 \pm .04	0.71 \pm .01
GRAPHLCP	0.67 \pm .03	0.61 \pm .03	0.73 \pm .01	0.66 \pm .02	0.70 \pm .02	0.76 \pm .01	0.72 \pm .02	0.73 \pm .01	0.70 \pm .02	0.76 \pm .01	0.64 \pm .03	0.68 \pm .03	0.75 \pm .01

global kernels, whereas larger values emphasize locality. Overall, performance is stable across this range, with intermediate values providing the best balance.

Initial densification threshold ($\tau_d^{(0)}$) Once we use automatic thresholding, γ controls the step size for iterative updates. With enough iterations T , performance is largely insensitive to γ ; empirically, $\gamma = 0.1$ ensures stable convergence. In contrast, the initial densification threshold $\tau_d^{(0)}$ has a stronger impact: lower values add more edges, while higher values restrict additions to highly similar nodes. This reduces noisy edges but could introduce bias.

We evaluate $\tau_d^{(0)} \in \{0.3, 0.5, 0.7, 0.9\}$ across 10 datasets. Figure 8 shows that the effect of the initial densification threshold depends on mean node homophily. For heterophilous graphs (e.g., WKB), lower thresholds improve coverage by compensating for weak topology. For homophilous graphs (e.g., ELC), higher thresholds reduce noise and improve coverage. Overall, $\tau_d^{(0)} = 0.5$ balances high coverage with favorably low prediction length.

A.8 More Conditional and Marginal Results

WSC results To have a more detailed picture of how we perform in comparison to the baselines, we show the full results of WSC in Tables 4 and 5. As previously discussed, GRAPHLCP attains a desirable trade-off between prediction length and coverage in comparison with other baselines, and this trade-off is clearer on the regression tasks.

Group-based conditional results We provide additional conditional coverage results for all four types of group-based conditional coverage in Figure 9.

Table 5: WSC prediction length results. GRAPHLCP yields shorter relative prediction lengths on regression tasks than on classification tasks. OOT (out-of-time) shows results attained after an unreasonably long time.

Method	ANH	CHI	EDU	ELC	INC	UNM	TWT	CMP	CRA	DBLP	CBAS	WKB	PMD
CaLLCP	2.31 \pm .26	2.33 \pm .09	2.62 \pm .14	1.10 \pm .03	2.49 \pm .08	2.17 \pm .07	2.54 \pm .14	OOT	2.27 \pm .10	OOT	1.20 \pm .14	4.14 \pm .08	1.47 \pm .03
SCP	1.66 \pm .09	1.94 \pm .07	2.02 \pm .10	1.01 \pm .03	1.94 \pm .07	1.81 \pm .04	2.10 \pm .07	1.03 \pm .04	0.91 \pm .04	1.40 \pm .06	1.99 \pm .10	3.09 \pm .34	1.22 \pm .02
NAPS	∞	∞	∞	∞	∞	∞	2.63 \pm .52	2.72 \pm .23	5.21 \pm .26	3.00 \pm .10	3.78 \pm .04	5.00 \pm .00	2.12 \pm .10
CF-GNN	1.82 \pm .22	1.67 \pm .14	1.88 \pm .12	0.85 \pm .02	1.80 \pm .07	1.61 \pm .05	2.26 \pm .07	3.67 \pm .60	1.52 \pm .33	2.00 \pm .25	2.55 \pm .27	3.78 \pm .24	1.40 \pm .21
SNAPS	1.72 \pm .09	1.91 \pm .04	2.13 \pm .03	1.22 \pm .03	1.94 \pm .04	1.74 \pm .04	∞	1.37 \pm .12	0.90 \pm .04	1.35 \pm .04	2.67 \pm .14	4.22 \pm .08	1.19 \pm .01
RLCP	1.66 \pm .09	1.91 \pm .07	2.02 \pm .10	1.01 \pm .03	1.94 \pm .07	1.81 \pm .04	2.10 \pm .07	1.06 \pm .05	0.90 \pm .04	1.38 \pm .06	2.05 \pm .07	3.06 \pm .33	1.22 \pm .02
GRAPHLCP	1.61 \pm .09	1.94 \pm .03	2.66 \pm .26	1.08 \pm .05	2.49 \pm .28	1.91 \pm .15	2.11 \pm .15	2.60 \pm .07	1.87 \pm .07	2.03 \pm .03	2.91 \pm .11	3.55 \pm .14	1.84 \pm .03

Table 6: Marginal prediction length. OOT (out-of-time) shows results attained after an unreasonably long time.

Method	ANH	CHI	EDU	ELC	INC	UNM	TWT	CMP	CRA	DBLP	CBAS	WKB	PMD
CaLLCP	2.24 \pm .28	2.15 \pm .06	2.24 \pm .14	1.06 \pm .02	2.12 \pm .08	2.13 \pm .06	2.54 \pm .13	OOT	2.89 \pm .09	OOT	2.83 \pm .03	4.59 \pm .03	1.15 \pm .01
SCP	1.66 \pm .09	1.94 \pm .07	2.02 \pm .10	1.01 \pm .03	1.94 \pm .07	1.81 \pm .04	2.10 \pm .07	1.08 \pm .01	0.98 \pm .01	1.16 \pm .01	1.92 \pm .03	4.26 \pm .10	1.09 \pm .00
NAPS	∞	∞	∞	∞	∞	∞	5.73 \pm 1.18	2.19 \pm .06	5.54 \pm .06	3.26 \pm .01	3.79 \pm .03	5.00 \pm .00	2.65 \pm .01
CF-GNN	1.82 \pm .22	1.67 \pm .14	1.88 \pm .12	0.85 \pm .02	1.80 \pm .07	1.61 \pm .05	2.26 \pm .07	3.56 \pm .63	1.55 \pm .26	1.82 \pm .25	2.40 \pm .29	4.41 \pm .15	1.30 \pm .13
SNAPS	1.72 \pm .09	1.91 \pm .04	2.13 \pm .03	1.22 \pm .03	1.94 \pm .04	1.74 \pm .04	∞	1.22 \pm .05	0.98 \pm .01	1.16 \pm .01	2.32 \pm .04	4.32 \pm .04	1.09 \pm .00
RLCP	1.66 \pm .09	1.91 \pm .07	2.02 \pm .10	1.01 \pm .03	1.94 \pm .07	1.81 \pm .04	2.10 \pm .07	1.08 \pm .01	0.98 \pm .01	1.16 \pm .01	1.92 \pm .03	4.24 \pm .10	1.09 \pm .00
GRAPHLCP	1.63 \pm .08	1.94 \pm .03	2.29 \pm .15	1.05 \pm .03	2.15 \pm .08	1.92 \pm .06	2.11 \pm .14	2.62 \pm .02	2.09 \pm .03	1.93 \pm .01	2.56 \pm .03	4.32 \pm .08	1.83 \pm .01

Marginal Prediction Length Table 6 shows the experimental results for the marginal prediction length over all datasets. Results show that vanilla SCP yields the smallest prediction length/size, while CaLLCP yields the largest. Also, (b) shows the performance across all datasets in more detail. Simultaneously looking at Table 1, CaLLCP most of the time over-covers, generating prediction sets that are larger than necessary.

A.9 Empirical runtime

We evaluate the wall-clock runtime of GRAPHLCP against SCP and RLCP on larger datasets. Results are in Table 7. As expected, GRAPHLCP is slower due to densification and PPR-based weighting. Despite this, runtime remains practical. Also, the thresholding step can keep the augmented graph sufficiently sparse, ensuring PPR computation remains scalable in practice. The results shown in the table are derived using the same hyperparameter used for the main results throughout the paper.

A.10 Datasets

We show the detailed statistics of all datasets in Table 8. We evaluate our proposed method across a diverse set of benchmark datasets across multiple domains and task types. For citation networks, we include Cora_ML (CRA), DBLP, and PubMed (PMD), while the Amazon co-purchase domain is represented by Computers (CMP). We utilize a set of geographic and transportation datasets for regression tasks, including Education (EDU), Election (ELC), Income (INC), Unemployment (UNM), Anaheim (ANH), and Chicago (CHI). Finally, we incorporate the Twitch (TWT) social network and finally GOOD-WebKB (WKB) and GOOD-CBAS (CBAS).

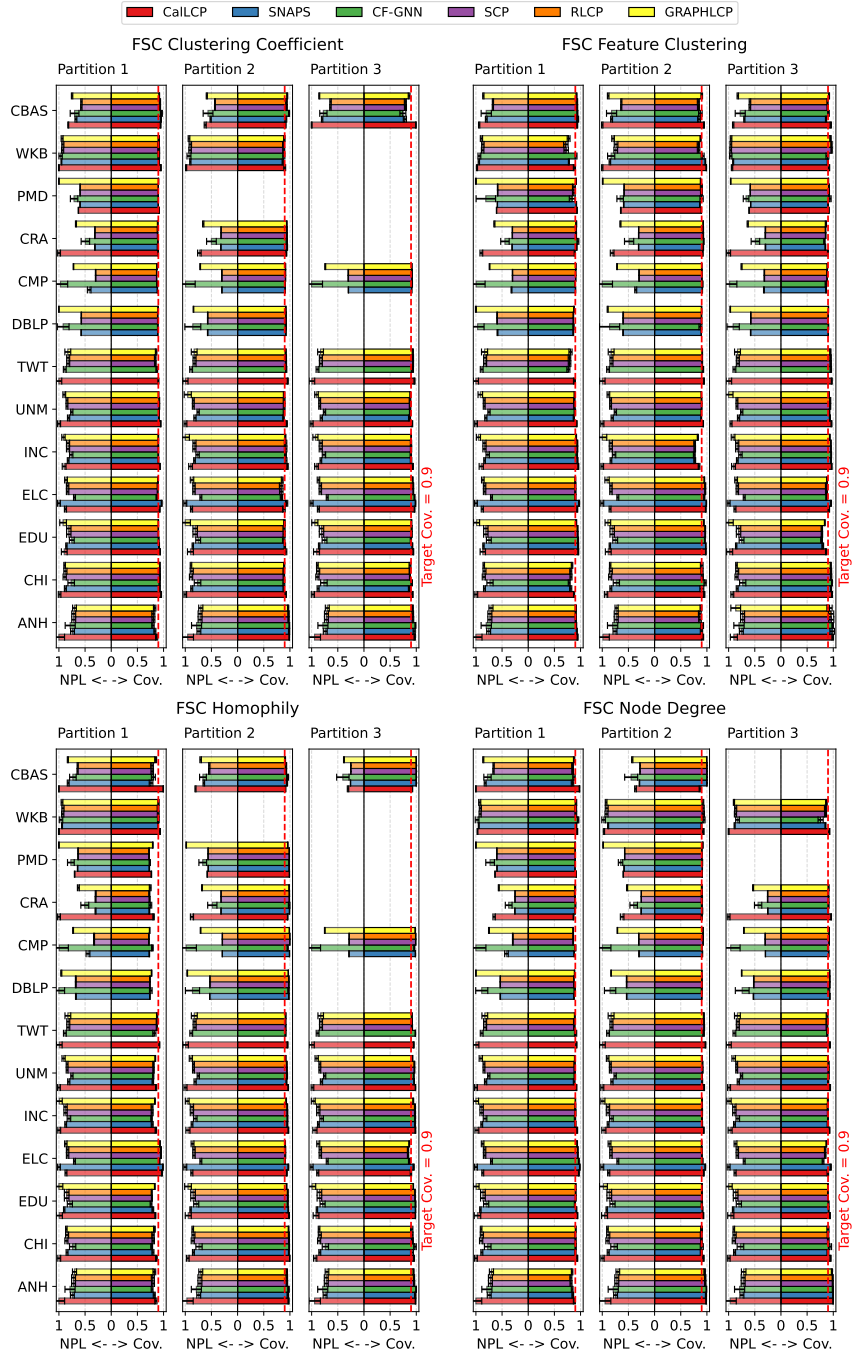


Figure 9: Results for group-based conditional coverage. It shows the minimum coverage across partitions for semantic and structural features where $\alpha = 0.1$. GRAPHLCP demonstrates superior coverage compared to baselines and more specifically in homophily and feature clustering.

Table 7: Wall-Clock Runtime on Larger Datasets (seconds)

Dataset	SCP	RLCP	GRAPHLCP
CMP	4.4	29.7	111.1
DBLP	7.5	28.3	508.8
PMD	9.2	30.7	145.2

Table 8: Dataset Statistics

Dataset	Domain	#Nodes	#Edges	#Features	#Classes
Cora_ML [3]	Citation	2,995	16,316	2,879	7
DBLP [3]	Citation	17,716	105,734	1,639	4
PubMed [3]	Citation	19,717	88,648	500	3
Computers [37]	Amazon	13,752	491,722	767	10
Education [20]	Geography	3,234	12,717	6	Reg.
Election [20]	Geography	3,234	12,717	6	Reg.
Income [20]	Geography	3,234	12,717	6	Reg.
Unemployment [20]	Geography	3,234	12,717	6	Reg.
Anaheim [20]	Transportation	914	3,881	4	Reg.
Chicago [20]	Transportation	2,176	15,104	4	Reg.
Twitch [20]	Social	1,912	31,299	3,170	Reg.
GOOD-WebKB [15]	OOD Benchmark	617	1138	1703	5
GOOD-CBAS [15]	OOD Benchmark	700	3962	4	4